ELSEVIER

Contents lists available at ScienceDirect

Journal of Alloys and Compounds

journal homepage: http://www.elsevier.com/locate/jalcom



Phase transformation and structure evolution of a Ti-45Al-7.5Nb alloy processed by high-pressure torsion



Xi Li ^{a, b}, Rian J. Dippenaar ^a, Jae-Kyung Han ^c, Megumi Kawasaki ^c, Klaus-Dieter Liss ^{d, e, a, b, *}

- ^a School of Mechanical, Materials, Mechatronic and Biomedical Engineering, University of Wollongong, Wollongong 2522, Australia
- ^b Australian Nuclear Science and Technology Organisation, Lucas Heights 2234, Australia
- ^c School of Mechanical, Industrial and Manufacturing Engineering, Oregon State University, Corvallis, OR 97331, USA
- d Materials and Engineering Science Program, Guangdong Technion Israel Institute of Technology, Shantou, Guangdong 515063, China
- ^e Technion Israel Institute of Technology, Haifa 32000, Israel

ARTICLE INFO

Article history:
Received 9 October 2018
Received in revised form
11 February 2019
Accepted 13 February 2019
Available online 14 February 2019

Keywords: Ti-Al alloys Order-disorder transition Heterogeneity Neutron diffraction High-pressure torsion

ABSTRACT

Intermetallic γ -based titanium aluminides of Ti-45Al-7.5Nb have been subjected to high-pressure torsion (HPT) processing. Significant grain refinement has been achieved from ~10 μ m to ~30 nm, leading to the improvement in both physical and mechanical properties. Complementary studies correlated the microstructure, phase transformation behavior and the enhancement of mechanical properties. Neutron and X-ray diffraction revealed that an ongoing order-disorder transformation occurs by HPT processing, resulting in large heterogeneous behavior between the surface-near and the median layers of the disk. While the γ -phase almost disappeared underneath the surface region, such order/disorder phase transformation consistently decreases towards the middle-thickness section of the samples. A low bulk texture index is consistent with grain rolling and swirling rather than slip deformation. Vickers microhardness indentation confirms the improvement of hardness from 308 H $_{\rm v}$ to 605 H $_{\rm v}$. For the first time, the present work demonstrates heterogeneity in structural transformation, such as displacive transformation and order/disorder transformation, which can be compared to earlier reported inhomogeneity in mechanical properties and microstructure within bulk nanostructured materials that were processed by HPT.

© 2019 Published by Elsevier B.V.

1. Introduction

Titanium aluminides are increasingly being developed as base materials for high-temperature aeronautic and aerospace applications because of their high strength-to-mass ratio in addition to their excellent corrosion resistance. For instance, both Rolls-Royce and General Electric identified titanium aluminides as candidate materials for turbine blades in jet engines [1]. Chladil et al. [2–4] demonstrated that γ -based Ti-Al intermetallics, highly alloyed with niobium, the so called TNB family, exhibit excellent specific yield strength and ductility. However, these alloys are brittle at room temperature. They consist of a *fcc*-based, ordered γ -phase, TiAl, of

L₁₀ structure and space group 123 of P 4/m m m and a hcp-based, ordered α₂-phase, Ti₃Al, of D0₁₉ structure and space group 194 of P 6_3 /m m c, which can further disorder to hcp α -Ti, a solid solution of same space group. The design of a processing route that will further improve plasticity and ductility of these TNB alloys remains a challenge to researchers and engineers. One possible approach to overcome this inherent brittle behavior is to reduce the grain size [5]. Processing by the application of severe plastic deformation is one suggested approach aimed at effective grain refinement [6]. Among the numerous severe processing deformation techniques, high-pressure torsion (HPT) is recognized as an effective grain refinement tool and the principles, on which this technique is based, are well documented elsewhere. Accordingly, earlier research has demonstrated that HPT processing can reduce the grain size of Ti-Al alloys to the micrometer or even nanometer scale [7–9]. By reference to the well-known Hall-Petch relationship [10], the yield strength will increase accordingly, although it has to be born in mind that this relationship breaks down at very small grain

^{*} Corresponding author. Materials and Engineering Science Program, Guangdong Technion - Israel Institute of Technology, Shantou, Guangdong 515063, China.

E-mail addresses: kdl@gtiit.edu.cn, kdliss@technion.ac.il, liss@kdliss.de (K.-D. Liss).

sizes. In addition, material with a nano-sized grain structure is likely to display superior plastic behavior, which prompted an assessment of the mechanical properties of selected HPT processed titanium aluminides in the present study. In earlier investigations, mechanical properties were assessed by Vickers micro-hardness measurements [9], while other researchers employed compression tests on micro-pillars [11] and nano-indentation measurements [12].

In addition to grain refinement, different research groups have provided convincing evidence of phase evolutions in the course of high-pressure torsion processing of Ti-Al alloys [7–9]. However, the details of the relevant phase changes occurring during processing are still a matter of debate and the role which strain is playing has not been resolved as yet. Korznikov et al. [7] reported that the γ phase in the HPT-treated Ti-Al alloys transforms to disordered states. Moreover, a fraction of the γ -phase transforms into α -phase, with a hexagonal close packed crystal structure. Kazantseva et al. [8] observed that the phase transformation occurs in Ti₃Al intermetallic compounds (α_2 -phase) by a shear mechanism under the application of high pressure. Conversely, Srinivasarao et al. [9] recently argued that high-pressure torsion does not produce an order/disorder phase transition in a γ -based Ti-Al alloy. Liss et al. [13] reported that a partial transformation of $\gamma \rightarrow \alpha_2/\alpha$ occurs under the influence of high pressure at room temperature despite the increase of volume per atom, driven by a large ordering energy in the γ -phase [14]. Our previous study, Han et al. [12], in which we used conventional X-ray diffraction analysis, pointed to a tendency towards the phase transformation $\gamma \rightarrow \alpha_2/\alpha$ in a Ti-45Nb-7.5Nb (at. %) alloy following HPT processing. However, the significance and the nature of this proposed phase change has not yet been established. Moreover, various apparently contradicting observations reveal the complexity of phase transitions in HPT-treated Ti-Al alloys. The fact that HPT processing produces highly anisotropic and inhomogeneous specimens needs to be taken into account for texture and mechanical testing on the severely deformed bulk materials [15,16].

X-ray and neutron diffraction techniques are commonly used to determine the phase composition and other crystallographic aspects in alloys, but for Cu-K_{α} X-ray diffraction, the penetration depth is absorption limited and is usually about 10 µm. Hence, this feature can be utilized to characterize different depths in a specimen upon layer-by-layer removal. However, it is difficult to distinguish between the ordered α_2 -and the disordered α -phase by X-ray diffraction. The weak superstructure reflections and a low α_2 phase fraction can hardly be distinguished from the background and statistical noise. On the contrary, neutron diffraction techniques pose advantages in the detection of order/disorder phase transitions, demonstrated by Watson et al. [17] as well as Kabra et al. [18], and recently reviewed by Liss [19]. The deep penetration depth of neutron diffraction enables bulk averaging and fast measurements [20-24]. For example, Watson et al. and Kabra et al. observed the order-disorder transition $\alpha_2 \rightarrow \alpha$ in Ti-43.9Al-4Nb-1Mo-0.1B (at. %) alloys and Ti-44Al-7Mo (at. %) alloys by in-situ neutron diffraction experiments during heating cycles [17,18]. By Cu- K_{α} X-ray diffraction techniques, we can determine compositional differences and phase fractions as a function of depth in a sample, by selective sectioning, while neutron diffraction allows for the detection of order/disorder phase transitions. Hence, these two techniques can be used in a complementary fashion to extract valuable crystallographic information [20].

The uncertainty about the exact mechanisms of the pertaining phase transformation and the concomitant induced microstructure during the HPT process in γ -based Ti-Al alloys prompted this study. Here, following Liss [25], we combine neutron scattering and X-ray

diffraction techniques to detect and quantify the crystallographic changes, thus clarifying the sequence of phase transformations and the pertaining micro-structural evolution as a function of the extent of deformation. In addition, scanning electron microscopy (SEM) and electron backscatter diffraction (EBSD) revealed further information on the pertaining microstructural development and finally, the increase in hardness as a result of grain refinement was assessed by Vickers micro-hardness measurements.

2. Experimental details

The Ti-45Al-7.5Nb alloy used in this investigation was produced through a powder metallurgical route, the powders being prepared by gas atomization, and then hot-isostatically pressed at 200 MPa at a temperature of 1553 K for 2 h [2]. Specimens were then machined into rods and cut into disks (10 mm diameter and 0.85 mm thick). An HPT facility [26], consisting of upper and lower anvils, illustrated in Fig. 1a, was used to process the as-received alloys. The sample disk is placed onto the lower anvil and then moved upwards until the disk was contained within the depressions of the two anvil surfaces. Each anvil has a circular depression of 0.25 mm in depth and 10 mm in diameter thereby providing a quasi-constrained state during processing [27]. A compressive force of 480 kN is applied to impose a pressure of 6 GPa onto the sample. Rotating the lower anvil in one direction at a fixed speed of 1 rpm imposes torsional strain and disk samples are strained in torsion for 5 and 10 turns respectively and are identified as follows (see Table 1):

- 0–0: The as-received material;
- 6–0: Sample subjected to a pressure of 6 GPa without torsional deformation:
- 6–5 and 6–10: Samples subjected to 5 and 10 turns of torsional strain under a pressure of 6 GPa, respectively.

The morphology, phase and texture of HPT-processed samples were assessed as shown in Fig. 1b. The microstructure of the disk surface was examined using SEM (JEOL NeoScope JCM-7001). The possibility of phase transitions during HPT processing was studied by using Cu-K $_{\alpha}$ X-ray diffraction (XRD) with wavelength (λ_{x}) of 1.5418 Å and wave-vector (k_{x}) of 4.0752 Å $^{-1}$ at both the University of Wollongong, Australia and Hanyang University, Korea. The focusing sizes were 1 mm \times 10 mm and 0.4 mm \times 12 mm (longitudinal \times transverse), respectively, both covering the disk diameter, thereby obtaining an average over the entire radial distribution.

X-ray diffraction (XRD) examinations were carried out both at the surface of the entire disk and the unveiled half mid-section (colored in red in Fig. 1b). Moreover, neutron diffraction was used to study the possible order/disorder transition during HPT processing in the Ti-Al alloy. Neutron diffraction was conducted on the high intensity neutron diffractometer WOMBAT [21] at the Australian Nuclear Science and Technology Organisation (ANSTO). A Ge-311 monochromator selected an incident beam wavelength $\lambda_n = 2.419 \,\text{Å}$ with corresponding wave number $k_n = 2.598 \,\text{Å}^{-1}$. The specimen-integrated crystallographic preferred orientation (texture) was measured in four-circle set-up employing righthanded Busing-Levy convention [28] at the WOMBAT neutron diffractometer. The samples 6-5 and 6–10 were rotated in tilt angle χ [29–31] of the sample from 0° to 90° in steps of 15° and around the ϕ -axis [29–31] by 360° in 73 steps of 4.9315°. Such odd number of steps allows for the probing of additional pole figure coverage as the Friedel symmetry is bypassed. The diffraction rings recorded by a 2-dimensional, cylindrical detector were sectored into three sectors in the detector azimuth η [29–31] of 5.25° each. The changes in hardness of the Ti-Al alloy following high-pressure

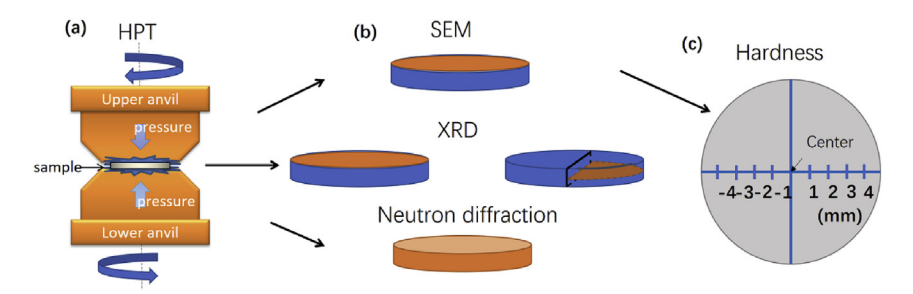


Fig. 1. Experimental processing of the Ti-Al alloys: (a) Schematic illustration of HPT processing of the Ti-Al alloy; (b) Different slices were used for morphology and structure characterization using both X-ray and neutron diffraction; (c) Hardness measurements.

Table 1Sample designation and processing parameters.

Sample	pressure [GPa]	torsion [turns]	Comments
0-0	0	0	as-received
6-0 6-5	6	0 5	pressurized HPT processed
6-10	6	10	HPT processed

torsion were determined by micro-hardness measurements. These measurements were made along the diameter on a polished plane close to the surface of each disk at positions, 1 mm apart as illustrated in Fig. 1c, using a LECO M-400-H1Vickers micro-hardness instrument with $100\,\mathrm{g}$ (0.98 N) loading and $12\,\mathrm{s}$ of indentation time.

3. Results and discussions

3.1. Microstructure

Back-scattered SEM images of the as-received sample and the disk edges following HPT processing are depicted in Fig. 2a–d. In Fig. 2a, the dark gray areas represent the γ -phase while the bright

regions show the α_2 -phase. The structure consists of a duplex microstructure containing equiaxed γ -phase with an average size of ~10 μm and parallel platelets of the γ - and α_2 -phases (the lamellar structure), which presumably formed at the eutectoid temperature T_{eu} [32,33]. The dark γ -phase and the bright α_2/α phase still exist as a duplex structure following HPT processing for 5 and 10 turns (Fig. 2b-d). Bending of the lamellae occurred along the shear direction by torsional straining around the peripheries of the disks. Comparison of the lamellar spacing of the α_2 -phase in the as-received condition (Fig. 2a) with that of the deformed specimens (Fig. 2b and c) provides convincing experimental evidence that HPT processing produces significant microstructural refinement. In some areas at the edge of sample 6–10, extreme grain refinement occurred, as shown in Fig. 2d, which we assume stem from originally large fully lamellar colony grain outliers and need further investigation.

3.2. Phase transformations during HPT processing

The X-ray attenuation length is $23.7 \,\mu m$ and the penetration depth $8.36 \,\mu m$ at 45° incidence based on the assumption that the density is $3860 \, kg/m^3$ and the weighted mass attenuation coefficient of the Ti-45Al-7.5Nb alloy is $10.95 \, m^2/kg$ (NIST database) [34].

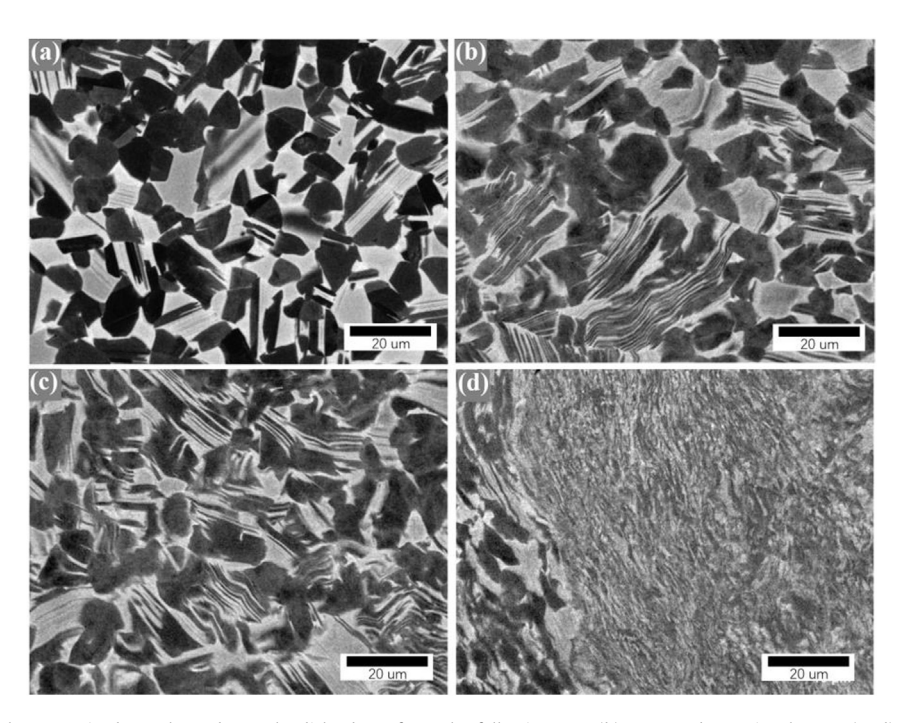


Fig. 2. Microstructure of (a) the as-received sample; and near the disk edges of samples following HPT: (b) 6 GPa and 5 torsional turns; (c-d) 6 GPa and 10 torsional turns.

Hence, X-ray diffraction can be used to average over a large specimen radius and characterize the average plastic strain within a thin layer below the measurement surface. The X-ray diffractograms obtained at the surface and the median layers of the samples following different HPT processing steps are compared in Fig. 3a. In this figure, the diffraction profiles with darker color refer to the surface plane and the brighter color to the median disk surface at each HPT step. The peaks of each sample were indexed by using the Crystallographic Information File (CIF, #1545053 and #1545054 for γ - and α_2 -phases, respectively) of the Crystallography Open Database [34] provided by Liss et al. [13]. The patterns of the asreceived samples, which are denoted as 'no treatment' in Fig. 3, consist of the peaks from the α_2/α - and γ -phases, thereby agreeing well with the SEM backscattering observations, as shown in Fig. 2a. Using the MAUD Rietveld analysis package [35], the phase fractions of the α_2/α_1 and α_2 -phases in the as-received samples at both the surface and the median layers were calculated as ~30 at. % and 70 at. %, respectively. Note our notation α_2/α for an ensemble of the ordered α_2 and disordered α phase, since X-rays cannot make a clear distinction between the two.

Salient features of the patterns obtained as a function of processing, are peak broadening and the evolution of the peak intensities. Increasing torsional deformation caused broadening of the X-ray diffraction peaks shown in Fig. 3a, indicating that the grains are being refined by deformation processing. By adopting an *isotropic* model where peak broadening is simplified, as being independent of the different *hkl* directions [36,37], the shape of the peak is described as a function of *size and strain* in MAUD [35]. The diffraction coherent crystallite sizes of the α_2/α -phase were 124, 92, 72 and 29 nm for samples 0-0, 6-0, 6-5 and 6-10, respectively, thereby providing convincing evidence that high-pressure torsion progressively reduces the crystallite size.

Following HPT processing, the grains are too small to measure the exact grain sizes from the SEM pictures shown in Fig. 2. In order to obtain a better estimate of the crystallite size, the Williamson-Hall method was employed to verify the crystallite size and internal strain in the median section of sample 6–10. The Williamson-Hall method assumes that a combination of size and strain contributes to the total breadth of a Bragg peak [38,39]. In this model, strain-induced peak broadening is assumed to result from crystal imperfections and distortion, expressed as $\varepsilon = \Delta Q_S/Q$. It is assumed that the grain size spreads homogeneously in reciprocal space by $\Delta Q_D = K \cdot 2\pi/D$, where K is a shape factor equal to 0.94 [40]. Then, the full width at half-maximum (ΔQ) is:

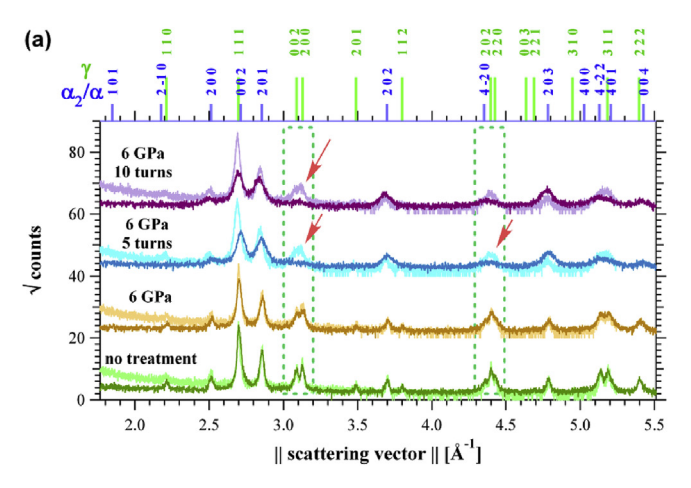
$$\Delta Q = (2\pi/D) \cdot K + \varepsilon Q \tag{1}$$

Using equation (1), the fitted ΔQ as a function of reciprocal space coordinate Q is depicted in Fig. 3b. Using the intercept of 0.0172 Å $^{-1}$, the grain size D is estimated as 34 nm. Moreover, the slope provides evidence of the existence of a highly stressed microstructure with an elastic strain of 0.0097. Such strain broadening is an overall average throughout the sampled volume, which can result from inter-granular stresses, interacting on the scale of the grain size as a local property, and from integration over a residual stress field, which would vary and hence, shift the peaks as a function of location. Note that strain and stress can be both positive and negative and must hold equilibrium over the specimen, so that compressive and expansional values may be half the total stress amplitude, if uniformly distributed.

By using a nano-indentation technique, Han et al. determined the Young's modulus of this material as 145 GPa and the yield strength as 2.35 GPa following 10 turns by HPT [12]. By using this modulus and our measured strain of 0.0097, we estimate a residual stress of 1.41 GPa. This value represents 61% of the reported yield point of this alloy and hence, only a small external stress of ~0.94 GPa is required to overcome the yield stress. Moreover, it can be argued that this stress amplitude is partly compressive, however, since the specimens are inhomogeneous, stress concentrations can be much higher and easily lead to crack formation and in the extreme, to mechanical failure.

By single peak fitting with a *Gaussian* function at the surfacenear layer, it transpires that the peak area of α_2/α -phase increases with processing, e.g. the α_2/α -202 X-ray peak area varies from 0.933 [counts Å⁻¹] in csample 6–0 to 2.676 [counts Å⁻¹] in sample 6–10. Similar trends are observed on the other main α_2/α peaks while the intensities of γ peaks largely shrink, providing convincing evidence that deformation by HPT increases the fraction of the α_2/α -phase at the expense of γ . Such behavior strongly underlines the notion that the disordered γ -phase transformation is driven by the high ordering energy of close-packed Ti-Al configurations [13,14].

It is important to note that the stress and strain distributions in the processed disks are far from being uniform, neither in the radial direction, expected by the principles of HPT [41], nor in the through-thickness direction as shown by the different hardness values [42]. For this reason, X-ray diffraction profiles taken at the macroscopic surface and the median section of the sample disks are expected to be different. Specifically, the present results indicate that the HPT-induced torsional plastic strain is higher at the sample



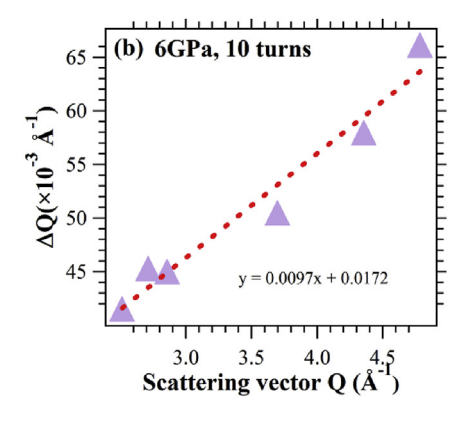


Fig. 3. (a) The XRD patterns of the samples before and after different HPT processes. The XRD patterns at surface and median layers of the disks were denoted as dark and light lines, respectively. (b) Williamson-Hall analysis for α_2/α at median layers of sample 6–10. The dashed line was fitted to data of each sample using equation (1).

surface than at the median section. Consequently, phase constituents would be different at the sample surface and at the median section as shown by a comparison between the purple and blue curves for the 6-5 and 6-10 samples as indicated by red arrows in Fig. 3a. The diffraction peaks of the γ -phase measured at the sample surface show progressively reduced intensity following torsion for 5 HPT turns and they eventually disappear with an increasing numbers of turns. Conversely the γ -phase peaks obtained from the mid-sections of the samples (lines with lighter color in Fig. 3a) are still present and largely broadened. The important conclusion from these observations is that the difference in the extent of severe plastic deformation from the center to the perimeter of a disk in this torsional experiment also influences the extent of the $\gamma \rightarrow \alpha_2/\alpha$ phase transition. It is therefore not surprising that some researchers observed this phase transition [7] and others did not [9]. It evidently depends on where in (or on) the specimen the phase fraction is determined.

Earlier research on two-phase materials, duplex stainless steel [43–47] and a Cu-Ag alloy [48] demonstrated that the HPT disks reveal unusual flow patterns involving double swirls and local vortices. The presence of swirls and vortices produced by HPT was explained by modelling the development of instabilities as a result of non-symmetrical shear and compressive stresses, especially when anvil misalignments increase [49]. These studies were conducted on the arbitrary-sectioned planes parallel to the HPT disk surfaces, but Kulagin et al. [50] have recently shown that shear is surface-parallel near the surface only. They have shown that turbulent flow may occur in the bulk volume, resulting in a rolling of vortices with localized areas of higher and reduced shear, as schematically shown in Fig. 4. Hence, severe plastic deformation occurs at or near the surface layers contacting the anvils, while inhomogeneous straining deep in the bulk (or disk thickness) eventually rolls off in a vortex-like manner. The result is that less transformed material is located next to highly deformed material in shear zones, leading to the observed differences between the diffractograms obtained from the near-surface region and the central layer respectively. These differences are attributed to the presence of two co-existing phases, which respond differently to torque in the shear-field of the matrix. The core of the vortices would experience less torsional shear [49] thus plastic deformation by HPT, while the interaction zone between neighbouring vortices suffers from enhanced severe plastic deformation. Therefore, the surface layer exhibits overall and homogeneously severe plastic deformation, while the bulk can contain highly as well as less severely plastically deformed regions. These observations in addition to taking into account the X-ray diffractograms, lead to the conclusion that the γ -phase is highly suppressed by severe plastic deformation. Considering that the γ -phase has the highest ordering energy of all Ti-Al intermetallic configurations [51], it would rather transform into the α_2/α -phase upon severe plastic deformation. Such transformation between the fcc- and the hcp-based phases

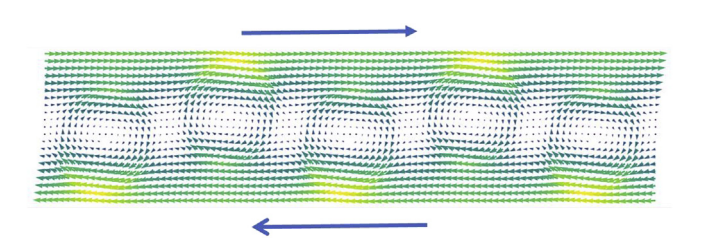


Fig. 4. Sketch of turbulent flow: Simple applied shear at the confined surfaces leads to a pure shear deformation thereunder while vortices can form, rolling in the bulk and separating shear zones (bands) from less deformed material, supported by evidence of Kulagin et al. [50].

occurs primarily displacively by changing the stacking sequence from ABCABC to ABABAB while no long-range diffusion occurs at the given temperature. Because the stoichiometry of the γ -phase (TiAl) is different from α_2 (Ti₃Al), the latter is supposed to be highly disordered. Similar disorder-driven $\gamma \rightarrow \alpha$ transformation has been observed upon the application of hydrostatic pressure even though the transformation-induced volume per atom increases and counterbalances the pressure-induced volume decrease [13].

Whereas X-rays have a penetration depth of only 10 µm, neutrons can penetrate much deeper and as a result, make it possible to obtain bulk information integrated over the entire specimen. It is peculiar that in the composition of the alloy under investigation, the disordered phases are close to a neutron scattering null matrix [19,52]. Thus, only peaks from the ordered α_2 -and γ -phases can be detected during neutron scattering experiments. The superstructure peak heights depend not only on the phase fraction, but also on the order parameter of each phase. Fig. 5a compares the neutron diffractograms of different samples before and after HPT processing. It shows that the diffraction peaks of both the α_2 -phase and the γ -phase broaden with increasing applied deformation strain by compression and concurrent torsion. Consistent with the X-ray evidence, the broadening of the neutron diffraction peaks indicates that the grains have been refined as a result of the high applied plastic strains.

The γ -001 diffraction peak, representing intermetallic order, is prominent and has a high intensity in the neutron diffraction pattern as indicated by a light green-dotted box in Fig. 5a, but it is almost non-existent in the X-ray diffractograms, which are shown in Fig. 3a. By contrast, the γ -111 as well as the γ -002/200 peaks have strong intensity in X-ray diffraction, Fig. 3a, whereas they are almost invisible to neutrons, as indicated by the green dotted box in Fig. 5a. This observation is fundamentally important because it allows a distinction to be made between ordered and disordered crystal structures through neutron diffraction experiments.

Specifically, an estimate of the total phase fractions can be made by X-ray diffraction analysis, while the extent to which a phase is ordered can be determined through the integrated neutron intensities (the area underneath a specific peak, for example the γ -001 peak). By single peak fitting using the Igor Pro 4 software, the relative areas underneath the γ -001 peak of samples 0-0, 6-0, 6-5, 6-10 were calculated as 0.013359, 0.009407, 0.006720 and 0.005923, respectively. The clear implication of this finding is that the fraction of the ordered γ -phase decreases with increasing applied strain through HPT processing. The relative areas underneath the α_2 -101 peaks of samples 0-0, 6-0, 6-5 and 6-10 as indicated by the blue box in Fig. 5a were 0.003534, 0.002497, 0.000932 and 0.0006232, hence showing the same trend. Neutron diffraction intensity ratios of the γ -001 and the α_2 -101 superstructure reflections normalized to the starting condition 0-0, and their ratios are shown in Fig. 5b. This peak area analysis shows that the fraction of the ordered α₂-phase decreases sharply following HPT processing. By comparison, the X-ray analysis indicated the application of severe plastic deformation that led to an increase in the fraction of the α_2/α -phase. Therefore, comparison between the neutron and Xray diffraction data leads to the conclusion that the ordered α_2 phase transforms into the disordered α -phase under the application of severe plastic deformation through HPT. This finding has important implications in the manufacturing of Ti-Al alloys since the disordered phase exhibits better ductility than the ordered

The X-ray diffraction patterns shown in Fig. 3a demonstrate that the γ -phase disappears and only the α_2/α -phase is observed on the surface of samples 6-5 and 6-10. On the other hand, the neutron diffractograms shown in Fig. 5a indicate that the bulk samples of 6-5 and 6-10 contain almost no ordered α_2 -phase. Therefore, the

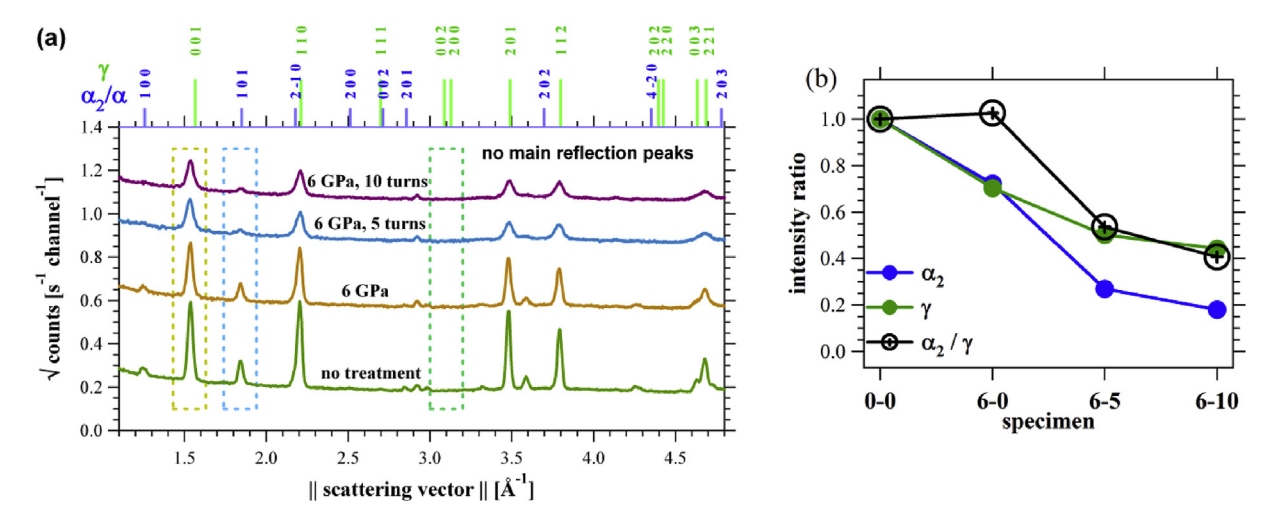


Fig. 5. (a) Neutron diffractograms of samples 0-0, 6-0, 6-5 and 6-10 using the WOMBAT instrument. Neutron diffraction intensity ratios of the γ -001 and the α_2 -101 superstructure reflections normalized to the starting condition 0-0, and (b) their ratios.

sequence of phase transformations on the surfaces of the samples following HPT is $(\alpha_2 + \gamma) \rightarrow (\alpha + \gamma) \rightarrow \alpha$. Conversely, the existence of both α_2/α -phase and γ -phase X-ray peaks at the half mid-section of samples 6-5 and 6–10 (both weaker lines in Fig. 3a) indicate that this phase transition is not fully completed at the median layer of the disk-shaped samples. Therefore, the extent to which phase transformations occur within HPT samples depends on the exact position within the sample.

3.3. Texture

In addition to the important aspects of microstructural development and phase evolution that result from severe plastic deformation, it is of the essence to determine the effect of such processing on crystal orientation. To this end, we used a four-circle neutron diffraction set-up to assess texture development integrated over the bulk. Fig. 6 shows the pole figures for the {001}- and {110}-lattice planes of the γ -phase for samples 6-5 (a,b) and 6-10 (c,d) respectively. Also shown is a schematic diagram of the preferred γ -crystal orientations (e). In both the torsionally-strained samples, a pronounced γ -110 type fiber texture is observed: Most of the {110} plane normals align along the cylinder axis of the sample while the {001} lattice plane normals are predominantly perpendicular to the cylindrical axis of the disk, as illustrated in Fig. 6e. This axial symmetry is the result of the axial-symmetry by compression straining and radial symmetry by torsional straining during HPT processing, when averaged over the entire specimen.

Bartels et al. [20,53] found a strongly modified cube texture in a γ -titanium aluminide in a rolling experiment, meaning that the crystallographic c-axis of the γ -phase is aligned with the transverse direction, which is perpendicular to both the shear and compression directions in a rolling process. In the case of torsional deformation, such as the case in the present investigation, any disk element at some radius from the center experiences well-defined shear and compressive straining, the transverse direction pointing radial, coinciding with the observed c-axis distribution (strictly speaking, the c^* plane normal). Therefore, we would expect local rolling texture if the position was resolved enough; however, sample averaging delivers the axial symmetry.

Compared to Fig. 6a and c shows that the intensity is equalized at the periphery of the pole figures, meaning that greater symmetry in the crystallographic orientations is achieved by 5 turns of HPT processing. It is also worth noting that the maximum texture

intensity is relatively low and decreases even further when the torsional deformation is increased to 10 turns. Deformation by crystallographic slip would result in strong texture maxima, while it is fairly weak in the present case, indicating that the main deformation mechanism changes from slip to grain boundary sliding as the grains are refined to the nanometer scale [54]. The important implication of this observation is that the weak texture is consistent with orientation randomization by the rolling of grains and vortices in a turbulent bulk flow as argued above in the section on X-ray diffraction. Thus, as opposed to deformation by dislocation slip, where grain rotation is terminated upon reaching a stable orientation with a zero Schmidt factor, particle rolling and grain boundary sliding continuously re-orient grains, thereby randomizing their orientations. These conclusions reached by the present texture analysis, are in excellent agreement with our earlier micromechanical study by nano-indentation. In that study, we have alluded to the role grain boundary sliding as a deformation mechanism by observing the increased strain rate sensitivity in the γ -based titanium aluminide after HPT processing [13]. Moreover, a recent review summarizing the available data on ultrafine-grained materials processed by severe plastic deformation, pointed to a consistent trend of increasing strain rate sensitivity with reducing grain size [55].

3.4. Microhardness measurement

Fig. 7 shows the experimentally determined micro-hardness values of samples 0-0, 6-0, 6-5 and 6-10. The shear strain applied is given by equation (2) below [56,57],

$$\gamma = \frac{2\pi N \cdot r}{h} \tag{2}$$

where N is the number of torsion turns, r is the radius in the disk, and h is the disk thickness. Equation (2) shows that the shear strain is a maximum at the edge of the disk and is zero at the center where r=0.

The hardness variations demonstrate an apparent hardness increase from 308 H_v to 337 H_v following the application of a compression force of 6 GPa without torsion straining. Because the compression induced phase change from γ to α_2/α [13] occurs displacively, stacking faults and ultrafine lamella hinder dislocation movement and thus increase the hardness, accompanied by

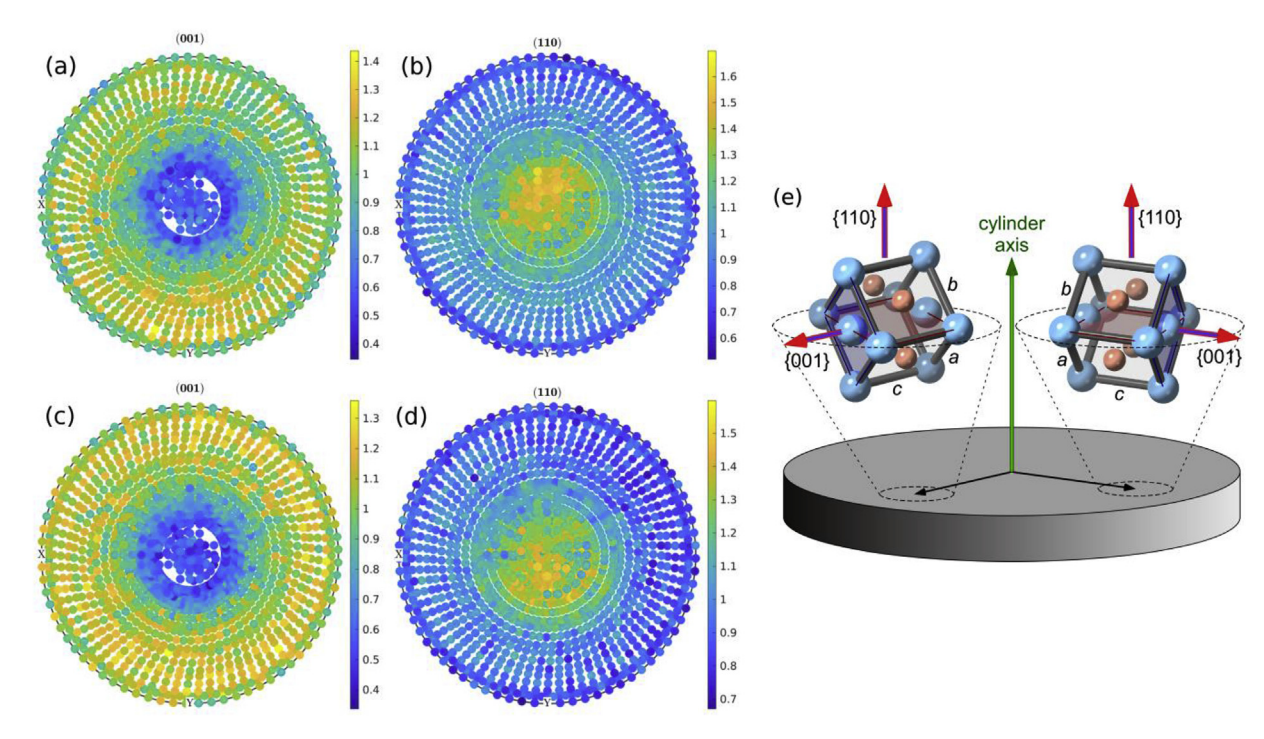


Fig. 6. Experimentally determined bulk-integrated texture of the γ -phase in the Ti-45Al-7.5Nb alloy after HPT process: 001-pole figure of sample 6-5 (a) and 6-10 (c); 110-pole figure of sample 6-5 (b) and 6-10 (d); and the preferred orientation of γ -phase using sample coordinate (e).

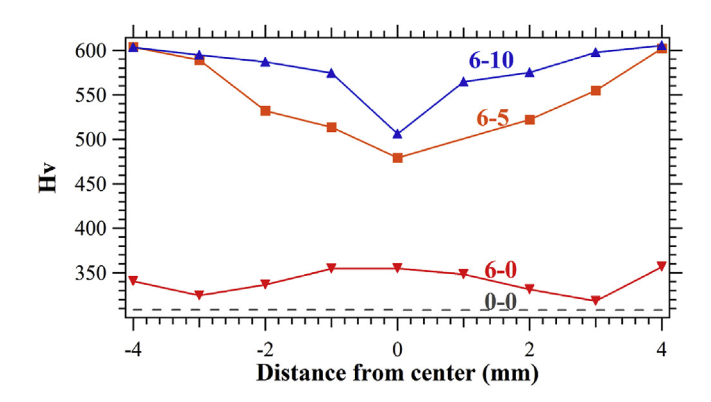


Fig. 7. Vickers micro-hardness with distance from the center of the disks after processing by HPT under 0, 5 and 10 revolutions of torsion at 6 GPa.

conventional dislocation hardening. Furthermore, the slight increase in hardness at the center of the disk and periphery is often observed at the compressive stage in the HPT procedure due to metal flow in a quasi-constrained manner [58]. Consistent with the trend in strain as shown in equation (2), the measured hardness increases from the center to the edge as a result of HPT processing (samples 6-5 and 6-10 in Fig. 7). The hardness increases to 337 $H_{\rm v}$ following the application of a compression force of 6 GPa without the application of torsion. It is attributed to displacive phase changes upon pressure loading, suggesting a high density of planar faults resulting in ultrafine lamellae on a nanometer scale. Specifically after 5 turns and 10 turns of torsion under a pressure of 6 GPa, the hardness increases to 480 and 510 H_v at the center and to 604 H_v at the edges of the disks, respectively. The hardness at the edge of the disk achieved the saturation level after 5 turns and the saturation value is twice as high as in the annealed condition.

The present hardness measurements taken close to the disk surface indicate that the hardness increase occurred in the absence of microstructural recovery [59]. An earlier review of hardness evolution models has shown that this particular hardness behavior is typical of materials processed at homologous temperatures of HPT processing below ~0.3 [42], which is the case in the present study for the γ -based titanium aluminide. Conversely, our earlier hardness measurements have shown that the saturated hardness is reached throughout the disk diameter even after 5 turns by HPT when testing at the mid-height of the disk [12]. This difference in the hardness behavior at different measuring planes in the through-thickness direction was first observed in Mg alloys [60-63] while it was not observed in pure Al due to the fast microstructural recovery during processing [60,63]. The heterogeneous distribution of hardness was observed in the throughthickness direction of steels [46,64-66], commercial purity Cu [67], pure Ag [68], and Ti alloy [69] disks following HPT processing. Moreover, a recent experiment demonstrated a clear heterogeneous grain size distribution leading to a gradient microstructure in an HPT-processed, interstitial free steel in the through-thickness direction [70]. These observed hardness heterogeneities have been attributed to flow localization and strain gradation: the former depends on the nature of the strain hardening of the material and the latter is due to the lateral friction between the samples and the anvil depression walls [71,72]. The present study demonstrates, for the first time, that heterogeneity exists not only in microstructure and mechanical properties, but also in order/ disorder transformation and phase transformations within the bulk sample subjected to severe plastic deformation applied by highpressure torsion.

4. Summary and conclusions

We have used advanced X-ray and neutron diffraction techniques in addition to microstructural analysis and hardness measurements for a comprehensive study of Ti-45Al-7.5Nb intermetallics. We correlated crystallographic transformations with

mechanical properties and microstructure.

- The application of severe plastic deformation to a Ti-45Al-7.5Nb alloy by high-pressure torsion results in the modification of a number of important microstructural features and hardness.
- The crystallite size is refined to 34 nm as the result of the application of high compressive pressure (6 GPa) and torsion (10 turns).
- The transformation of the material in the near-surface region is much more pronounced than in the median layer which may be caused by the higher plastic strain at the surface and the heterogeneous deformation process.
- The sequence of phase transformations at the surface is: $(\alpha_2 + \gamma) \rightarrow (\alpha + \gamma) \rightarrow \alpha$.
- This sequence of events is not fully realized at the median layer of the thin disk.
- An order-disorder phase transition occurs during high-pressure torsional deformation.
- Following high-pressure torsion processing, a {110} type of fiber texture is formed in the γ-phase, integrated over the bulk.
- The hardness is increased from 308 H_V to a maximum of 605 H_V.
- High residual stresses remain in the room-temperature processed material with values close to the yield strength limit, making the processed specimen susceptible to brittle failure.

The combination of X-ray analysis and neutron diffraction techniques in the present investigation paves the way for the extension of the present study of Ti-Al intermetallics to other alloy systems where order/disorder phase transitions occur.

Acknowledgements

The authors gratefully acknowledge the award of a China Scholarship Council (CSC) grant to Xi Li. We also acknowledge financial support of and access to experimental facilities of the University of Wollongong, the Hanyang University and the Australian Nuclear Science and Technology Organisation (ANSTO), under proposal P6022. This study was supported in part by the National Science Foundation United States under Grant No. DMR-1810343.

References

- [1] B.P. Bewlay, S. Nag, A. Suzuki, M.J. Weimer, TiAl alloys in commercial aircraft engines, Mater. A. T. High. Temp. 33 (4–5) (2016) 549–559.
- [2] H. Chladil, H. Clemens, H. Leitner, A. Bartels, R. Gerling, F.-P. Schimansky, S. Kremmer, Phase transformations in high niobium and carbon containing γ-TiAl based alloys, Intermetallics 14 (10) (2006) 1194–1198.
- [3] H. Chladil, H. Clemens, G.A. Zickler, M. Takeyama, E. Kozeschnik, A. Bartels, T. Buslaps, R. Gerling, S. Kremmer, L. Yeoh, Experimental studies and thermodynamic simulation of phase transformations in high Nb containing γ-TiAl based alloys, Int. J. Mater. Res. 98 (11) (2007) 1131–1137.
- [4] F. Appel, M. Oehring, J. Paul, A novel in situ composite structure in TiAl alloys, Mater. Sci. Eng., A 493 (1) (2008) 232–236.
- [5] F. Froes, C. Suryanarayana, G.-H. Chen, A. Frefer, G.R. Hyde, Nanostructure processing for titanium-based materials, JOM J. Miner. Metals Mater. Soc. 44 (5) (1992) 26–29.
- [6] R.Z. Valiev, T.G. Langdon, Principles of equal-channel angular pressing as a processing tool for grain refinement, Prog. Mater. Sci. 51 (7) (2006) 881–981, https://doi.org/10.1016/j.pmatsci.2006.02.003.
- [7] A. Korznikov, O. Dimitrov, G. Korznikova, J. Dallas, A. Quivy, R. Valiev, A. Mukherjee, Nanocrystalline structure and phase transformation of the intermetallic compound TiAl processed by severe plastic deformation, Nanostruct. Mater. 11 (1) (1999) 17–23.
- [8] N. Kazantseva, N. Mushnikov, A. Popov, P. Terent'ev, V. Pilyugin, Severe plastic deformation and hydrogenation of the titanium aluminides, J. Alloys Compd. 509 (38) (2011) 9307—9311.
- [9] B. Srinivasarao, A. Zhilyaev, R. Muñoz-Moreno, M. Pérez-Prado, Effect of high pressure torsion on the microstructure evolution of a gamma Ti-45Al-2Nb-2Mn-0.8 vol% TiB₂ alloy, J. Mater. Sci. 48 (13) (2013) 4599-4605.

- [10] N. Hansen, Hall—Petch relation and boundary strengthening, Scr. Mater. 51 (8) (2004) 801–806.
- [11] K. Edalati, S. Toh, H. Iwaoka, M. Watanabe, Z. Horita, D. Kashioka, K. Kishida, H. Inui, Ultrahigh strength and high plasticity in TiAl intermetallics with bimodal grain structure and nanotwins, Scr. Mater. 67 (10) (2012) 814–817, https://doi.org/10.1016/j.scriptamat.2012.07.030.
- [12] J.-K. Han, X. Li, R. Dippenaar, K.-D. Liss, M. Kawasaki, Microscopic plastic response in a bulk nano-structured TiAl intermetallic compound processed by high-pressure torsion, Mater. Sci. Eng., A 714 (2018) 84–92, https://doi.org/ 10.1016/j.msea.2017.12.065.
- [13] K.-D. Liss, K.-I. Funakoshi, R. Dippenaar, Y. Higo, A. Shiro, M. Reid, H. Suzuki, T. Shobu, K. Akita, Hydrostatic compression behavior and high-pressure stabilized β-phase in γ-based titanium aluminide intermetallics, Metals 6 (7) (2016) 165, https://doi.org/10.3390/met6070165.
- [14] M. Asta, D. de Fontaine, M. Van Schilfgaarde, First-principles study of phase stability of Ti–Al intermetallic compounds, J. Mater. Res. 8 (10) (1993) 2554–2568.
- [15] O. Bouaziz, Y. Brechet, J.D. Embury, Heterogeneous and architectured materials: a possible strategy for design of structural materials, Adv. Eng. Mater. 10 (1-2) (2008) 24–36.
- [16] H.-J. Lee, S.K. Lee, K.H. Jung, G.A. Lee, B. Ahn, M. Kawasaki, T.G. Langdon, Evolution in hardness and texture of a ZK60A magnesium alloy processed by high-pressure torsion. Mater. Sci. Eng., A 630 (2015) 90–98.
- high-pressure torsion, Mater. Sci. Eng., A 630 (2015) 90–98.

 [17] I.J. Watson, K.D. Liss, H. Clemens, W. Wallgram, T. Schmoelzer, T.C. Hansen, M. Reid, In situ characterization of a Nb and Mo containing γ-TiAl based alloy using neutron diffraction and high-temperature microscopy, Adv. Eng. Mater. 11 (11) (2009) 932–937.
- [18] S. Kabra, K. Yan, S. Mayer, T. Schmoelzer, M. Reid, R. Dippenaar, H. Clemens, K.-D. Liss, Phase transition and ordering behavior of ternary Ti–Al–Mo alloys using in-situ neutron diffraction, Int. J. Mater. Res. 102 (6) (2011) 697–702.
- [19] K.-D. Liss, Metals challenged by neutron and synchrotron radiation, Metals 7 (12) (2017) 266, https://doi.org/10.3390/met7070266.
- [20] K.-D. Liss, A. Bartels, A. Schreyer, H. Clemens, High-energy X-rays: a tool for advanced bulk investigations in materials science and physics, Textures Microstruct. 35 (3–4) (2003) 219–252.
- [21] G.E. Bacon, K. Lonsdale, Neutron diffraction, Rep. Prog. Phys. 16 (1) (1953) 1.
- [22] W. Reimers, A.R. Kaysser-Pyzalla, A. Schreyer, H. Clemens, Neutrons and Synchrotron Radiation in Engineering Materials Science: from Fundamentals to Material and Component Characterization, John Wiley & Sons, 2008.
- [23] V. Stefan, N. Dimitar, B. Anatoly, K. Denis, P. Peter, X-ray and neutron diffraction of TiAl alloys, Math. Nat. Sci. (2015) 78.
- [24] T. Schmoelzer, K.-D. Liss, G.A. Zickler, I.J. Watson, L.M. Droessler, W. Wallgram, T. Buslaps, A. Studer, H. Clemens, Phase fractions, transition and ordering temperatures in TiAl–Nb–Mo alloys: an in-and ex-situ study, Intermetallics 18 (8) (2010) 1544–1552.
- [25] K.-D. Liss, Quantum beam science—applications to probe or influence matter and materials, Quant. Beam Sci. 1 (1) (2017) 1, https://doi.org/10.3390/ qubs1010001.
- [26] M. Kawasaki, J.-i. Jang, Micro-mechanical response of an Al-Mg hybrid system synthesized by high-pressure torsion, Materials 10 (6) (2017) 596.
- [27] R.B. Figueiredo, P.R. Cetlin, T.G. Langdon, Using finite element modeling to examine the flow processes in quasi-constrained high-pressure torsion, Mater. Sci. Eng., A 528 (28) (2011) 8198–8204.
- [28] W.R. Busing, H.A. Levy, Angle calculations for 3-and 4-circle X-ray and neutron diffractometers, Acta Crystallogr. 22 (4) (1967) 457–464.
- [29] D. Chateigner, Combined Analysis, John Wiley & Sons, 2010.
- [30] J. Grasslin, L.B. McCusker, C. Baerlocher, F. Gozzo, B. Schmitt, L. Lutterotti, Advances in exploiting preferred orientation in the structure analysis of polycrystalline materials, J. Appl. Crystallogr. 46 (1) (2012) 173–180.
- [31] H.-R. Wenk, Neutron diffraction texture analysis, Rev. Mineral. Geochem. 63 (1) (2006) 399–426.
- [32] F. Appel, R. Wagner, Microstructure and deformation of two-phase γ -titanium aluminides, Mater. Sci. Eng. R Rep. 22 (5) (1998) 187–268, https://doi.org/10.1016/S0927-796X(97)00018-1.
- [33] R. Ramanujan, Phase transformations in γ based titanium aluminides, Int. Mater. Rev. 45 (6) (2000) 217–240.
- [34] S. Gražulis, A. Daškevič, A. Merkys, D. Chateigner, L. Lutterotti, M. Quirós, N.R. Serebryanaya, P. Moeck, R.T. Downs, A. Le Bail, Crystallography Open Database (COD): an open-access collection of crystal structures and platform for world-wide collaboration, Nucleic Acids Res. 40 (D1) (2012) D420–D427, https://doi.org/10.1093/nar/gkr900.
- [35] L. Lutterotti, S. Matthies, H. Wenk, MAUD (Material Analysis Using Diffraction): a User Friendly Java Program for Rietveld Texture Analysis and More, Proceeding of the Twelfth International Conference on Textures of Materials (ICOTOM-12), NRC Research Press, Ottawa, Canada, 1999, p. 1599.
- [36] I. Lonardelli, Deformation Mechanisms in Bulk Nanostructured Aluminum Obtained after Cryomilling and Consolidation by Spark Plasma Sintering, University of Trento, 2010.
- [37] D. Balzar, N. Audebrand, M. Daymond, A. Fitch, A. Hewat, J. Langford, A. Le Bail, D. Louër, O. Masson, C. McCowan, Size-strain line-broadening analysis of the ceria round-robin sample, J. Appl. Crystallogr. 37 (6) (2004) 911–924.
- [38] G. Williamson, W. Hall, X-ray line broadening from filed aluminium and wolfram, Acta Metall. 1 (1) (1953) 22—31.
- [39] E.J. Mittemeijer, U. Welzel, The "state of the art" of the diffraction analysis of crystallite size and lattice strain, Z. Krist. Int. J. Struct. Phys. Chem. Asp. Cryst.

- Mater. 223 (9) (2008) 552-560.
- [40] A. Patterson, The Scherrer formula for X-ray particle size determination, Phys. Rev. 56 (10) (1939) 978–982.
- [41] A.P. Zhilyaev, T.G. Langdon, Using high-pressure torsion for metal processing: fundamentals and applications, Prog. Mater. Sci. 53 (6) (2008) 893–979, https://doi.org/10.1016/j.pmatsci.2008.03.002.
- [42] M. Kawasaki, Different models of hardness evolution in ultrafine-grained materials processed by high-pressure torsion, J. Mater. Sci. 49 (1) (2014) 18–34.
- [43] Y. Cao, M. Kawasaki, Y. Wang, S. Alhajeri, X. Liao, W. Zheng, S. Ringer, Y. Zhu, T. Langdon, Unusual macroscopic shearing patterns observed in metals processed by high-pressure torsion, J. Mater. Sci. 45 (17) (2010) 4545–4553.
- [44] Y. Cao, Y. Wang, R. Figueiredo, L. Chang, X. Liao, M. Kawasaki, W. Zheng, S. Ringer, T. Langdon, Y. Zhu, Three-dimensional shear-strain patterns induced by high-pressure torsion and their impact on hardness evolution, Acta Mater. 59 (10) (2011) 3903—3914.
- [45] Y. Cao, Y. Wang, S. Alhajeri, X. Liao, W. Zheng, S. Ringer, T. Langdon, Y. Zhu, A visualization of shear strain in processing by high-pressure torsion, J. Mater. Sci. 45 (3) (2010) 765.
- [46] Y. Huang, M. Kawasaki, T.G. Langdon, An investigation of flow patterns and hardness distributions using different anvil alignments in high-pressure torsion. I. Mater. Sci. 48 (13) (2013) 4533–4542.
- [47] Y. Huang, M. Kawasaki, T.G. Langdon, Influence of anvil alignment on shearing patterns in high-pressure torsion, Adv. Eng. Mater. 15 (8) (2013) 747–755.
- [48] Y. Tian, X. An, S. Wu, Z. Zhang, R.B. Figueiredo, N. Gao, T. Langdon, Direct observations of microstructural evolution in a two-phase Cu–Ag alloy processed by high-pressure torsion, Scr. Mater. 63 (1) (2010) 65–68.
- [49] Y. Huang, M. Kawasaki, T.G. Langdon, An evaluation of the shearing patterns introduced by different anvil alignments in high-pressure torsion, J. Mater. Sci. 49 (8) (2014) 3146–3157.
- [50] R. Kulagin, Y. Beygelzimer, Y. Ivanisenko, A. Mazilkin, H. Hahn, High pressure torsion: from laminar flow to turbulence, in: IOP Conference Series: Materials Science and Engineering, vol. 194, IOP Publishing, 2017, 012045.
- [51] J. Zou, C.L. Fu, M.H. Yoo, Phase stability of intermetallics in the Al Ti system: a first-principles total-energy investigation, Intermetallics 3 (4) (1995) 265–269, https://doi.org/10.1016/0966-9795(95)97286-A.
- [52] T. Okuchi, A. Hoshikawa, T. Ishigaki, Forge-hardened TiZr null-matrix alloy for neutron scattering under extreme conditions, Metals 5 (4) (2015) 2340–2350.
- [53] A. Bartels, H. Kestler, H. Clemens, Deformation behavior of differently processed γ-titanium aluminides, Mater. Sci. Eng., A 329 (2002) 153–162.
- [54] M. Pérez-Prado, G. González-Doncel, O. Ruano, T. McNelley, Texture analysis of the transition from slip to grain boundary sliding in a discontinuously recrystallized superplastic aluminum alloy, Acta Mater. 49 (12) (2001) 2259–2268.
- [55] M. Kawasaki, B. Ahn, P. Kumar, J.i. Jang, T.G. Langdon, Nano-and micro-mechanical properties of ultrafine-grained materials processed by severe plastic deformation techniques, Adv. Eng. Mater. 19 (1) (2017) 1600578.
- [56] R. Valiev, Y.V. Ivanisenko, E. Rauch, B. Baudelet, Structure and deformation behaviour of Armco iron subjected to severe plastic deformation, Acta Mater. 44 (12) (1996) 4705–4712.

- [57] F. Wetscher, A. Vorhauer, R. Stock, R. Pippan, Structural refinement of low alloyed steels during severe plastic deformation, Mater. Sci. Eng., A 387 (2004) 809–816.
- [58] Y. Song, E.Y. Yoon, D.J. Lee, J.H. Lee, H.S. Kim, Mechanical properties of copper after compression stage of high-pressure torsion, Mater. Sci. Eng., A 528 (13–14) (2011) 4840–4844.
- [59] M. Kawasaki, B. Ahn, T.G. Langdon, Significance of strain reversals in a twophase alloy processed by high-pressure torsion, Mater. Sci. Eng., A 527 (26) (2010) 7008-7016.
- [60] M. Kawasaki, R.B. Figueiredo, T.G. Langdon, An investigation of hardness homogeneity throughout disks processed by high-pressure torsion, Acta Mater. 59 (1) (2011) 308–316, https://doi.org/10.1016/j.actamat.2010.09.034.
- [61] R.B. Figueiredo, M.T.P. Aguilar, P.R. Cetlin, T.G. Langdon, Deformation heterogeneity on the cross-sectional planes of a magnesium alloy processed by high-pressure torsion, Metall. Mater. Trans. A 42A (10) (2011) 3013–3021.
- [62] R.B. Figueiredo, T.G. Langdon, Development of structural heterogeneities in a magnesium alloy processed by high-pressure torsion, Mater. Sci. Eng., A 528 (13–14) (2011) 4500–4506.
- [63] M. Kawasaki, R.B. Figueiredo, T.G. Langdon, Twenty-five years of severe plastic deformation: recent developments in evaluating the degree of homogeneity through the thickness of disks processed by high-pressure torsion, J. Mater. Sci. 47 (22) (2012) 7719–7725.
- [64] A. Hohenwarter, A. Bachmaier, B. Gludovatz, S. Scheriau, R. Pippan, Technical parameters affecting grain refinement by high pressure torsion, Int. J. Mater. Res. 100 (12) (2009) 1653–1661.
- [65] Y. Song, W. Wang, D. Gao, E.Y. Yoon, D.J. Lee, C.S. Lee, H.S. Kim, Hardness and microstructure of interstitial free steels in the early stage of high-pressure torsion, J. Mater. Sci. 48 (13) (2013) 4698–4704.
- [66] M.S. Matoso, R.B. Figueiredo, M. Kawasaki, D.B. Santos, T.G. Langdon, Processing a twinning-induced plasticity steel by high-pressure torsion, Scr. Mater. 67 (7–8) (2012) 649–652.
- [67] H.J. Jeong, E.Y. Yoon, D.J. Lee, N.J. Kim, S. Lee, H.S. Kim, Nanoindentation analysis for local properties of ultrafine grained copper processed by high pressure torsion, J. Mater. Sci. 47 (22) (2012) 7828–7834.
- [68] Z. Hegedűs, J. Gubicza, M. Kawasaki, N.Q. Chinh, J.L. Lábár, T.G. Langdon, Stability of the ultrafine-grained microstructure in silver processed by ECAP and HPT, J. Mater. Sci. 48 (13) (2013) 4637–4645.
- [69] M. Nakai, M. Niinomi, J. Hieda, H. Yilmazer, Y. Todaka, Heterogeneous grain refinement of biomedical Ti–29Nb–13Ta–4.6Zr alloy through high-pressure torsion, Sci. Iran. 20 (3) (2013) 1067–1070, https://doi.org/10.1016/ iscient.2013.01.004.
- [70] J.Y. Kang, J.G. Kim, H.W. Park, H.S. Kim, Multiscale architectured materials with composition and grain size gradients manufactured using high-pressure torsion, Sci. Rep. 6 (2016) 26590.
- [71] R.B. Figueiredo, G.C. de Faria, P.R. Cetlin, T.G. Langdon, Three-dimensional analysis of plastic flow during high-pressure torsion, J. Mater. Sci. 48 (13) (2013) 4524–4532.
- [72] R.B. Figueiredo, M.T.P. Aguilar, P.R. Cetlin, T.G. Langdon, Analysis of plastic flow during high-pressure torsion, J. Mater. Sci. 47 (22) (2012) 7807–7814.